AIChE

Effect of Supercritical Deposition Synthesis on Dibenzothiophene Hydrodesulfurization Over $NiMo/Al_2O_3$ Nanocatalyst

Mehrdad Alibouri
Catalysis Research Center, Research Institute of Petroleum Industry, Tehran 18745-4163, Iran; and
Dept. of Chemical Engineering, Isfahan University of Technology, Isfahan 84156-83111, Iran

Seyyed M. Ghoreishi
Dept. of Chemical Engineering, Isfahan University of Technology, Isfahan 84156-83111, Iran

Hamid R. Aghabozorg
Catalysis Research Center, Research Institute of Petroleum Industry, Tehran 18745-4163, Iran

DOI 10.1002/aic.11867
Published online July 13, 2009 in Wiley InterScience (www.interscience.wiley.com).

The synthesis of two $NiMo/Al_2O_3$ catalysts by the supercritical carbon dioxide/methanol deposition (NiMo-SCF) and the conventional method of wet coimpregnation (NiMo-IMP) were conducted. The results of the physical and chemical characterization techniques (adsorption–desorption of nitrogen, oxygen chemisorption, XRD, TPR, TEM, and EDAX) for the NiMo-SCF and NiMo-IMP demonstrated high and uniform dispersed deposition of Ni and Mo on the Al_2O_3 support for the newly developed catalyst. The hydrodesulfurization (HDS) of fuel model compound, dibenzothiophene, was used in the evaluation of the NiMo-SCF catalyst vs. the commercial catalyst (NiMo-COM). Higher conversion for the NiMo-SCF catalyst was obtained. The kinetic analysis of the reaction data was carried out to calculate the reaction rate constant of the synthesized and commercial catalysts in the temperature rang of 543–603 K. Analysis of the experimental data using Arrhenius' law resulted in the calculation of frequency factor and activation energy of the HDS for the two catalysts. © 2009 American Institute of Chemical Engineers *AIChE J,* 55: 2665–2674, 2009
Keywords: supercritical deposition, $NiMo/Al_2O_3$, hydrodesulfurization, dibenzothiophene

Introduction

Hydrodesulfurization (HDS) is a key process used in producing clean engine fuels. In the process, alumina supported CoMoS, NiMoS, and NiWS phases are traditionally used as catalysts. The various classes of sulfur compounds are in the middle distillate fraction having different alkyl substitutions in positions 4 and 6 on the dibenzothiophene (DBT) ring, are known as refractory compounds, which are the most resistant to HDS.[1,2] Because of new stringent environmental restrictions on the sulfur content of diesel fuel, many attempts have been made to improve the catalysts activity of HDS process.[3,4] In this sense, the threshold limit for sulfur in diesel fuel is expected to be regulated to 50 ppm of weight (ppmw) or less within the next few years.[5] To meet the specifications, refineries need to increase the conversion in their HDS processes and requires catalysts that are more active than those currently used. To improve the catalytic

Correspondence concerning this article should be addressed to S. M. Ghoreishi at ghoreshi@cc.iut.ac.ir

activity several approaches have been taken, of which the search for new active phases, supports and catalysts synthesis methods has been particularly noticeable.

The catalyst preparation method also had an effect on the HDS activity. The conventional method for the preparation of Mo supported catalysts on silica or alumina is the incipient wetness impregnation with an ammonium heptamolybdate solution, followed by calcination and sulfidation.[6–8] Many researches have been recently carried out in this regard such as sol-gel, incipient wetness impregnation/coimpregnation,[9] equilibrium deposition filtration (EDF),[10] and thermal spreading.[11]

Nowadays, it is well known that catalytic behavior (activity and selectivity) of molybdenum-based HDS catalysts strongly depends on the dispersion of the Mo surface species. Recently, nanoparticles with high dispersion and surface area supported on different support materials are currently used extensively as catalysts for chemical transformations. The surface of the nanoparticles plays an important role in their catalytic properties. The surface atoms are chemically more active compared to the bulk atoms because they usually have fewer adjacent coordinate atoms and unsaturated sites or more dangling bonds.[12,13]

Supercritical fluid (SCF) deposition is an alternative and promising way to deposit metal nanoparticles onto the surfaces of porous solid supports with high dispersion.[14–19] Supercritical deposition involves the dissolution of an organometallic precursor in a SCF and the impregnation of the substrate by exposure to this solution. Subsequent treatment of the impregnated substrate results in metal/substrate nanocomposites. Erkey and coworkers. have successfully synthesized supported platinum and ruthenium nanoparticles with particle size as small as 1 nm and metal content as high as 40 wt % on a wide range of materials.[20–22] High-resolution TEM micrographs showed a good distribution of highly dispersed platinum and ruthenium particles throughout the bulk of all the supports used.

Compared with conventional liquid solvents, the low surface tension of SCFs not only permit better penetration to the pores and wetting of the pores than liquid solvents, but also avoid the pore collapse which can be occurred on certain structures such as organic and silica aerogels by liquid solvents. Among the SCFs, supercritical carbon dioxide (SC-CO_2), readily accessible with a T_c of 304 K and a P_c of 73.8 bars, is particularly attractive since it is abundant, inexpensive, nonflammable, nontoxic, and environmentally benign and leaves no residue in the treated medium.[23]

It is known that inorganic salts are generally not soluble in SC-CO_2 because CO_2 is nonpolar. However, entrainers may be employed to increase solubility and conductivity in SC-CO_2, for example, (i) addition of small amounts of polar fluids as a cosolvent (e.g., water, methanol, ethanol, and acetone[24,25]), (ii) use of a salt with a large hydrophobic cation and anion (e.g., alkylammonium + tetraphenylborate[26]), (iii) use of a fluorinated ion for increased solubility (e.g., tetra(*p*-fluorophenyl)borate[27]), or (iv) a combination of the above.

To improve the activity of the catalyst in the HDS of DBT, the preparation of $NiMo/Al_2O_3$ catalyst was carried out in this study by supercritical carbon dioxide impregnation (NiMo-SCF). The newly developed catalyst was characterized by different physical and chemical methods and its characteristics were compared with those of prepared catalyst via wet coimpregnation (NiMo-IMP). The activity of NiMo-SCF was evaluated in the HDS process using a fixed bed reactor and compared with commercial catalyst (NiMo-COM).

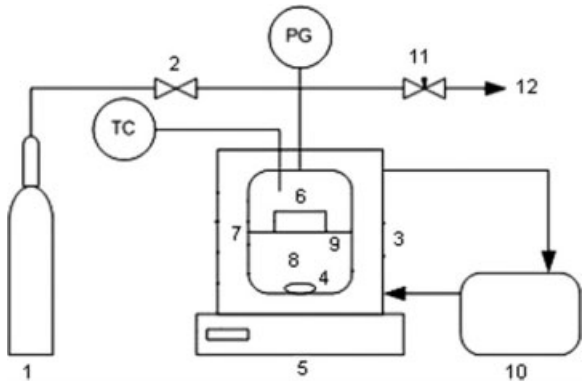

Figure 1. The experimental set-up for SC-CO_2 deposition.

1, CO_2 cylinder; 2, valve; 3, bath; 4, magnetic stirrer; 5, stirrer; 6, basket; 7, vessel; 8, solution; 9, screen; 10, circulating heater and cooler; 11, needle valve; 12, vent.

Experimental

Catalyst preparation

In preparation of the catalyst, one metal complex compound and one metal salt as the source of catalytic metal and promoter were used: molybdenum hexacarbonyl ($Mo(CO)_6$) and nickel nitrate ($Ni(NO_3)_2{\cdot}6H_2O$). Due to the much better solubility and phase behavior of $Mo(CO)_6$ in SC-CO_2[28] with respect to $(NH_4)_6Mo_7O_{24}$, thus in this study $Mo(CO)_6$ was chosen as the main source of molybdenum to provide active sites of the catalyst. As the source of catalyst promoter, $Ni(NO_3)_2.6H_2O$ was used but because of its insolubility in SC-CO_2, 6 wt % methanol was utilized as an entrainer, which can significantly enhance the solvation power of SC-CO_2.

The experimental set-up used in the synthesis of the catalyst is shown in Figure 1. With crushing and sieving, the commercial Al_2O_3 support was prepared with the mesh sizes of 18 and 35 (0.5–1.0 mm particle diameter). The prepared Al_2O_3 commercial support was then placed into a basket made out of stainless steel, and then the basket was placed into a high-pressure vessel (internal volume of 60 cm^3) equipped with a stirring bar together with suitable amount of $Ni(NO_3)_2 \cdot 6H_2O$ (Fluka 99%), $Mo(CO)_6$ (Merck 99%), and methanol (Merck 99.5%). The vessel was sealed and cooled to the 283 K using a bath circulator and charged with CO_2 (65 bar). Subsequently, the vessel was heated to 353 K using the bath circulator; higher temperature increased the pressure of the CO_2 inside the vessel and then using a needle valve the pressure was set and controlled at 276 bars. The operating conditions of SCF (353 K, 276 bars) were maintained for a period of 24 h and then the vessel was depressurized. After cooling the vessel to ambient temperature, the basket was removed. The samples were dried at 333 K overnight

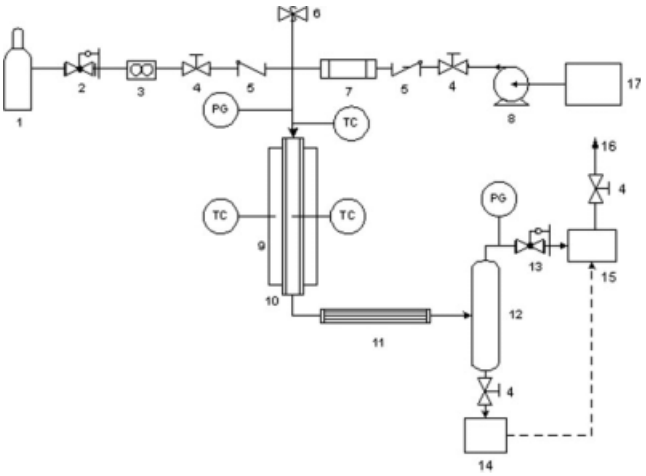

Figure 2. Schematic of flow fixed bed reactor.

1, H_2 cylinder; 2, pressure reducer; 3, mass flow meter; 4, screw-down valve; 5, check valve; 6, relief valve; 7, evaporator; 8, pump; 9, furnace; 10, reactor; 11, condenser; 12, separator; 13, back pressure regulator; 14, liquid trap; 15, GC; 16, vent; 17, liquid feed; TC, thermocouple; PG, pressure gauge.

and calcined in air at 823 K for 3 h. The metal content of the prepared catalyst (NiMo-SCF) was determined using atomic absorption technique (3.2 wt % Ni and 8.2 wt % Mo). A conventional catalyst (NiMo-IMP; 3.1 wt % Ni and 8.3 wt % Mo) with Al_2O_3 commercial support (0.5–1.0 mm particle diameter) was synthesized via wet coimpregnation of ammonium heptamolybdate (Aldrich, 99.98%) and nickel nitrate hexahydrate (Fulka 99%). The impregnated samples were dried at 60°C overnight and calcined in air at 550°C for 3 h. The commercial catalyst (2.2 wt % Ni and 9.3 wt % Mo) used in this study supplied as extrudates. With crushing and sieving, the commercial catalyst (NiMo-COM) sample was prepared with the same mesh sizes 18 and 35 comparable with the synthesized catalyst of this study.

Catalyst evaluation

Two catalysts (NiMo-SCF and NiMo-COM) were evaluated in a laboratory scale fixed bed flow reactor shown in Figure 2. This apparatus provides a high pressure and temperature continuous flow reactor. The stainless steel 316 tubular reactor was custom designed with 50 cm length, 0.94 cm internal diameter, and wall thickness of 0.17 cm. It is housed in a tubular electric furnace capable of heating up to 1073 K. A high-pressure syringe pump (ISCO, Model 260D) was used to pump the liquid hydrocarbon feed into the reactor against hydrogen pressure. During operation, the pump liquid storage cylinder was kept at a constant temperature of 273 K using a cooling tape. This led to a better control and reliability of the hydrocarbon flow rate. Evaporator vaporized the liquid before it was charged into the reactor. Hydrogen flow rate was measured and controlled using a Brooks mass flow meter. A back pressure regulator was used to maintain the overall system pressure required for HDS. Temperature in the reactor was monitored and maintained using two thermocouples. The first was used to control the temperature of the tubular furnace. The second is connected to the tubular reactor such that its tip was always at the center of the catalyst bed. All temperature measurements reported in this study refer to the temperature measured by the reactor thermocouple.

Two model hydrocarbon feeds were used in this study: (1) *n*-heptane (Merck, >99%) + dibenzothiophene (DBT, Aldrich, >99%), and (2) *n*-heptane + toluene (Aldrich, >99.5%) + DBT. The DBT concentration in the fuel was 0.5 wt %. For each run, to avoid hot spots, 0.50 g of catalyst was diluted with Silicon carbide (SiC, 60 mesh) to a constant volume of 1.5 cm^3 before being charged into the reactor. Silicon carbide of particle diameter 0.25 mm was used to enclose the catalyst bed at both ends in the reactor. Before the performance test, the catalysts were sulfided in situ with a solution of 3 wt % carbon disulfide (CS_2, Aldrich, >99%) in cyclohexane (Aldrich, >99%) at 573 K and 20 bars for 4 h. Upon reaching system steady state after 4 h, the reaction effluents were condensed and analyzed by a gas chromatograph (Model 8700 Perkin–Elmer) using a fused silica capillary column (15 m) with a temperature program from 373 to 523 K (10 K min^{-1}). The temperature range, pressure, H_2/feed ratio, and weight hourly space velocity (WHSV) for the HDS reaction were 543–603 K, 20 bar, 800 Nm^3/m^3, and 45 h^{-1}, respectively. All measurements in this study were triplicated with the reproducibility of ±2.6% standard deviation.

The reaction scheme for DBT desulfurization is shown in Figure 3. It has been proposed[29,30] that the reaction proceeds in accordance with the hydrogenolysis pathway, through the direct desulfurization route (DDS), leading to the production of biphenyl (BP), or by a second hydrogenation reaction pathway (HYD), in which one of the aromatic rings of DBT is firstly prehydrogenated, forming tetrahydrodibenzothiophene and hexahydrodibenzothiophene, which is later desulfurized to form cyclohexylbenzene (CHB).

To apply the appropriate assumption for the experimental reactor in regard to mass transfer mechanism, it is necessary to investigate the actual geometrical conditions of the reactor and catalyst. While catalyst particles of 0.5–1.0 mm diameter were shown to have minimal mass transfer limitations, some studies[31,32] has shown that when catalyst particles are sandwiched between smaller particles of an inert material, it could be assumed that the effective catalyst particle diameter is that of the smaller material. The importance of the aspect ratio and axial convective diffusion parameters for acceptable evaluation of hydroprocessing catalysts has been

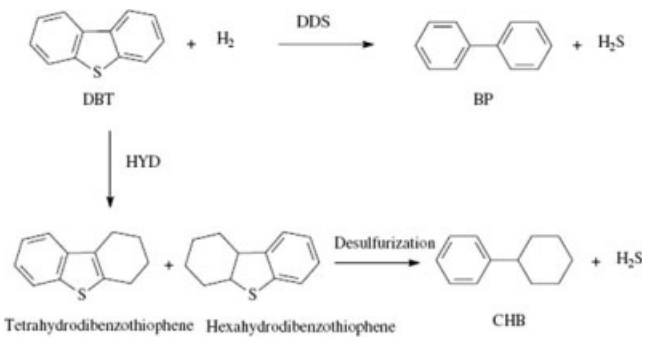

Figure 3. Reaction path network for HDS of DBT.

Table 1. Reactor and Catalyst Evaluation Parameters

Parameter	Aspect Ratio (Reactor Internal Diameter/Catalyst Particle Diameter)	Axial Convective Diffusion Parameter (Reactor Length/Catalyst Particle Diameter)
Minimum	25.0	50
This study	37.6	86

explained.[31] Table 1 presents the minimum and actual values of this study for these parameters recommended.[31] The aspect ratio and axial convective diffusion parameters for the catalyst particles used in this study exceed the minimum recommended values by 1.5 and 1.7 times, respectively. It is clear from Table 1 that the present study has used acceptable catalyst evaluation conditions.

For the synthesized and commercial catalysts, the main products of the reaction were BP and CHB. Based on the conversion and selectivity data, utilizing the pseudo first order rate equation with respect to DBT,[7,33–36] and convective mass transfer mechanism (neglecting axial dispersion coefficient: $D_z \rightarrow 0$ or in other words, $N_{Pec} \rightarrow \infty$), the reaction rate constant of HDS (k_{HDS}) was calculated according to the one-dimensional axial mass balance equation for the plug flow reactor:

$$k_{HDS} = -\frac{F}{W}\ln(1-X) \tag{1}$$

$$k_{HDS} = k_o \exp\left[-\frac{E}{RT}\right] \tag{2}$$

where F is the feed rate of DBT (mol/min), W is the catalyst weight (g), X is the mole fractional conversion of DBT, k_o is the frequency factor (mol/g cat. min) and E is the activation energy (J/mol). Hydrogenolysis (DDS) and hydrogenation (HYD) overall selectivity was calculated according to the formula:

$$S_o = \frac{X_{CHB}}{X_{BP}} \tag{3}$$

Characterization methods

The nitrogen adsorption–desorption isotherms were determined on an ASAP 2000 Micromeritics equipment. Before the experiments, the samples were degassed at 573 K in vacuum for 2 h. The volume of the adsorbed N_2 was normalized to the standard temperature and pressure. Specific surface area (S_{BET}) was calculated by the BET equation applied to the range of relative pressures $0.05 < P/P_0 < 0.20$. The average pore diameter was calculated by applying the Barret-Joyner-Halenda method (BJH) to the adsorption branches of the N_2 isotherms. The cumulative pore volume was obtained from the isotherms at $P/P_0 = 0.99$.

Oxygen pulse chemisorptions were used to characterize the dispersion of MoS_2 on the catalysts. An automated catalyst characterization unit (Autosorb 2321) was used for the chemisorptions measurement. The samples were pretreated in hydrogen at 523 K for 2 h before oxygen chemisorptions. Oxygen chemisorptions isotherms were obtained at 298 K.

The X-ray patterns were recorded on a PHILIPS PW1840 diffractometer using a monochromatic Cu Ka radiation. The TPR experiments of catalysts were carried out in a semiautomatic Micromeritics TPD/TPR 2900 apparatus interfaced to a microcomputer. TPR profiles were obtained by passing a 5% H_2/Ar flow (50 ml/min) through the sample. The temperature was increased at a rate of 10 K/min, and the amount of H_2 consumed was determined with a thermoconductivity detector (TCD). The effluent gas was passed through a cold trap before the TCD to remove water from the exit stream.

Transmission electron microscopy (TEM) was used to determine the dispersion of nickel and molybdenum on the support. Sample slurry was prepared via dispersion in ethanol. The powders in the solution were deposited on a grid with a holy carbon copper film. After drying, the samples were transferred to a PHILIPS CM200 FEG (Field Emission Gun) instrument with 200 kV of acceleration voltage for transmission electron microscopy test. The metal content of the prepared catalyst was determined using atomic absorption technique (Perkin–Elmer Model AAnalyst 200).

Results and Discussion

Catalyst characterization

The pore textural parameters, such as the specific area (S_{BET}), cumulative pore volume (V_p), average pore diameter (D_p) of supports and catalysts, and oxygen uptake of sulfided prepared catalysts via supercritical impregnation (NiMo-SCF) and wet coimpregnation (NiMo-IMP) are listed in Table 2. The BET surface area, pore volume and BJH average pores diameter of Al_2O_3 support after incorporation via supercritical deposition slightly decreased with respect to commercial support about 14.6%, 10.8%, and 3.0% respectively. But, the dispersion of the Ni and Mo species for NiMo-IMP results in significant decreasing the BET surface area (30.5%) and pore volume (24.3%) as shown in Table 2. It is imperative to realize that the decrease in the surface area and pore volume of support by using conventional impregnation method is significant in comparison to supercritical deposition which is also obtained in other studies.[37–40]

Dispersion of the active phase plays an important role in catalysis. Catalysis is a surface phenomenon and typically only the fraction of the active phase exposed on the support surface is important and responsible for catalytic activity. This is described and quantified by dispersion. In this study, oxygen chemisorptions were conducted on the catalysts synthesized by supercritical deposition and conventional method and the results are shown in Table 2. The results

Table 2. Pore Textural Parameters of Support and Catalysts and Oxygen Chemisorption Data of MoS_2 Catalysts

Sample	S_{BET} ($m^2\ g^{-1}$)	V_p ($cm^3\ g^{-1}$)[a]	D_p (nm)[b]	Oxygen Uptake (mol/g cat.)
Al_2O_3	295	0.37	5.07	–
NiMo-SCF	252	0.33	4.92	97
NiMo-IMP	205	0.28	4.65	83

[a]V_p at $P/P_0 = 0.99$.
[b]Calculated by BJH method.

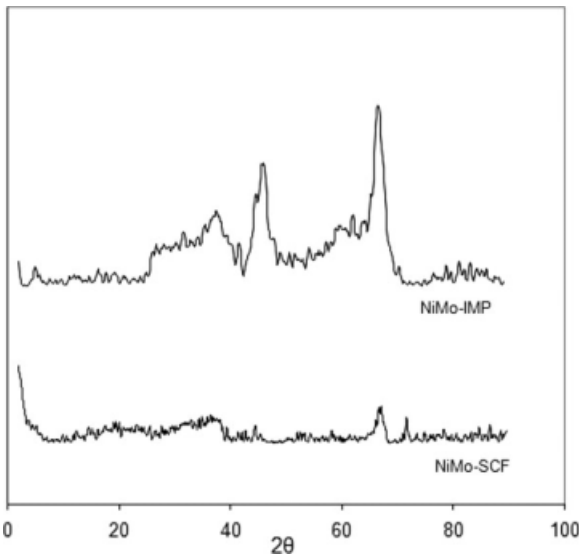

Figure 4. X-ray patterns of the oxided NiMo-SCF and NiMo-IMP catalysts.

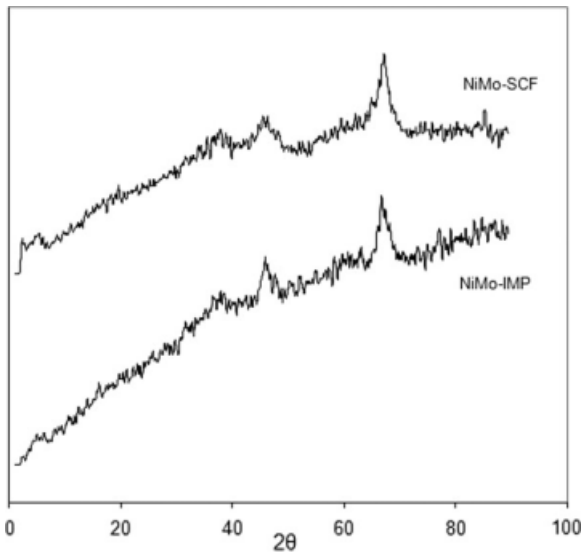

Figure 5. X-ray patterns of the sulfided NiMo-SCF and NiMo-IMP catalysts.

demonstrate that the oxygen uptake for the synthesized catalyst by supercritical deposition is higher than the synthesized conventional catalyst.

The observed phenomena are due to low surface tension of SCFs which not only permits better penetration into the pores than liquid solvents, but also avoids the pore collapse and agglomeration of Mo and Ni species. Overall one can conclude that there is a major improvement in the dispersion of the active phases of the catalyst on the Al_2O_3 support using supercritical deposition in comparison with conventional impregnations methods.

Figure 4 shows the XRD patterns of the prepared NiMo-SCF catalyst and NiMo-IMP catalyst. As observed in Figure 4, no reflections belonging to molybdenum oxides are realized and the observed reflection for nickel oxides is also very weak. Contrary to the obtained results for NiMo-SCF, the Figure 4 shows some reflections for the NiMo-IMP catalyst which is the indication of larger particle size for the two metals. The X-ray of NiMo-SCF and NiMo-IMP catalysts were taken and the results are shown in Figure 5. Molybdenum sulfide is expected to have their most intense reflections at 2θ values of 14.4° (d value = 0.614 nm). None of this was, however, detected in the patterns for the NiMo-SCF and NiMo-IMP catalysts as shown in Figure 5. This is not unexpected since the MoS_2 is poorly crystalline and its most intense X-ray reflections are barely visible even in unsupported MoS_2.[41]

Thus one can conclude that the observed phenomenon deviating the two catalysts in terms of produced particle size is due to fact that the smaller sized metal particles deposit in the pores of the support and, therefore, can not be detected as specific strong reflections as shown for the NiMo-SCF in Figure 4. It is imperative to realize that the method of metal deposition via supercritical impregnation can be pinpointed as the most significant and effective variable in the formation of highly dispersed Ni and Mo oxide phases inside the support pores due to special properties of SCFs in terms of low surface tension and viscosity and higher diffusion rate. These special properties of SCFs permit the dispersed deposition of metallic salts on the support surface and avoid the agglomeration of particles in contrast to liquid solvents in the conventional method.

The TPR curves of the NiMo-SCF and NiMo-IMP catalysts in the oxide form and of bulk MoO_3 are shown in Figure 6. The TPR profile of the bulk MoO_3 contains two reduction peaks at 1036 and 1163 K,[42] which correspond to the two-steps reduction of MoO_3 ($MoO_3 \rightarrow MoO_2 \rightarrow Mo^0$).[43–45] A significant decrease in the reduction temperature is observed when MoO_3 oxide is used in the catalyst support. As shown in Figure 6, the TPR profile of the NiMo-SCF catalyst contains three peaks at 692 K (low temperature), 824 K (medium temperature) and 965 K (high temperature). These peaks are in accordance with the Mo_I, Ni_I, and $Mo_{II} + Ni_{II}$ peaks respectively.[46] The low temperature peak

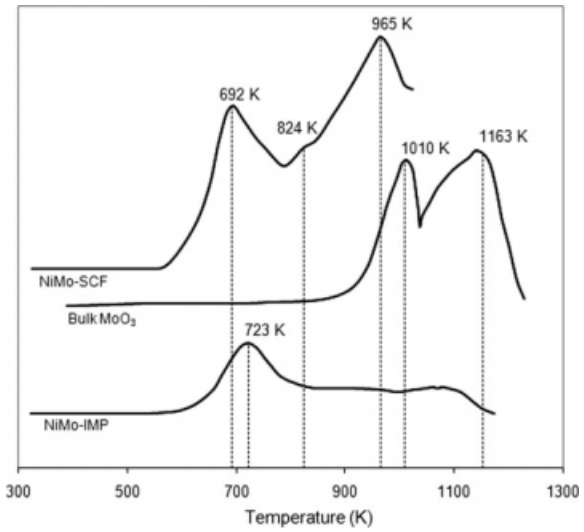

Figure 6. TPR curves of the NiMo-SCF and NiMo-IMP catalysts and of bulk MoO_3.

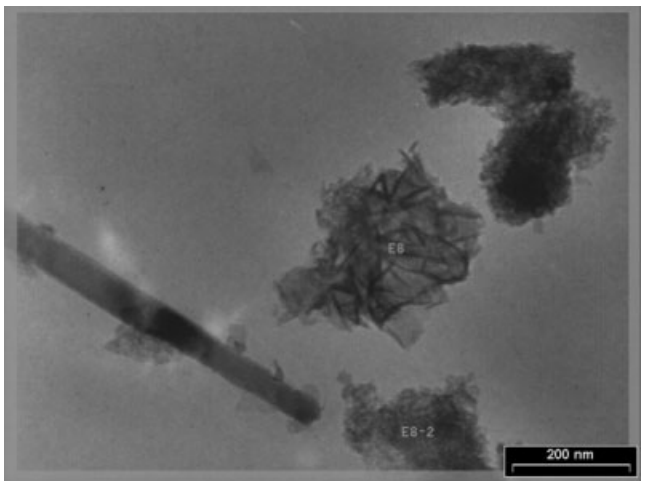

Figure 7. TEM micrograph of the sulfided NiMo-SCF catalyst (E8 and E8-2 points).

is generally associated with the reduction of Mo^{6+} to Mo^{4+} of polymeric octahedral Mo species (Mo_I)[47,48] while the medium temperature peak corresponds to the reduction of octahedrally coordinated Ni^{2+} species (Ni_I) weakly bound to the surface.[49] The high temperature peak may be assigned to the peak of (Mo_{II} + Ni_{II}). The Ni_{II} peak is identified with bulk-like $NiAl_2O_4$,[50] whereas the Mo_{II} peak can be ascribed to the second step in the reduction of the polymeric octahedral Mo species (from Mo^{4+} to Mo^0) or to the first step of reduction of isolated tetrahedral Mo^{6+} species in strong interaction with the support.[48,51] A broad peak is observed in the range of 773–1163 K for the conventional catalyst. It should be mentioned that the intensity of main reduction peak in NiMo-SCF catalyst is high compared with the TPR profiles of NiMo-IMP catalyst. Comparing the TPR of NiMo-SCF with NiMo-IMP catalyst and other TPR profile in literature[52] indicates that the reduction of Ni and Mo species in supported catalyst synthesized via supercritical deposition occurs at lower temperatures. The better reduction behavior of catalyst synthesized via supercritical deposition is due to

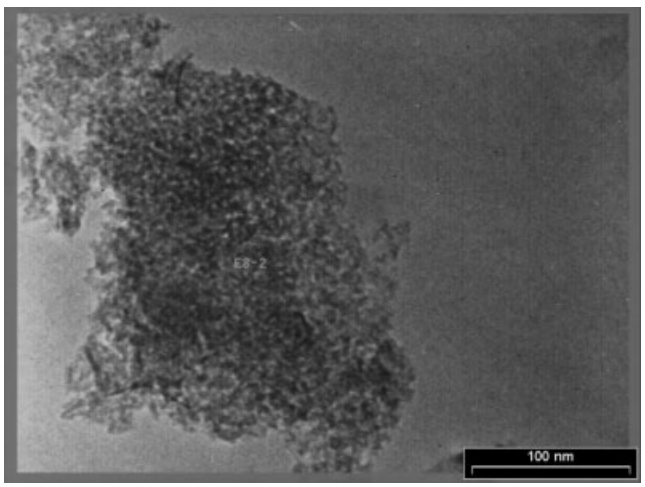

Figure 8. TEM micrograph of the sulfided NiMo-SCF catalyst (E8-2 point).

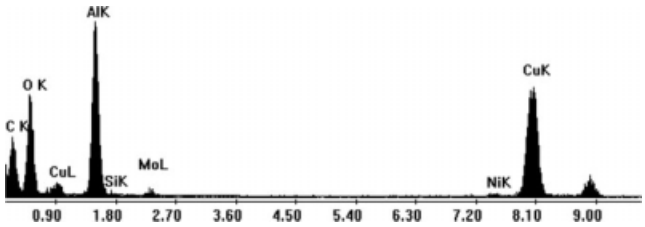

Figure 9. EDAX spectrum of E8 point of the NiMo-SCF catalyst (Figure 7).

the increase in the dispersion of Mo and Ni oxide species into Al_2O_3 support.

In addition to other analyses, the sulfided catalyst used in this study was also characterized using TEM. The main objective for the TEM studies was to determine the dispersion of MoS_2 in the Al_2O_3 supported catalyst. Despite several sample preparation methods, the Al_2O_3 supported catalyst could not be anchored to the grids well enough to allow the electron beam to focus and image the catalyst at high magnification. At high magnification, focusing the electron beam on the Al_2O_3 supported catalyst resulted in rapid movement of the Al_2O_3 supported catalyst, thus preventing its effective imaging. Therefore, due to the aforementioned obstacles, MoS_2 particles can not be appreciated in Figures 7 and 8, corresponding images of the sulfided catalyst prepared using the supercritical deposition method. Thus, to obtain evidence of the uniform dispersed deposition of active phase in the Al_2O_3 supported catalyst via supercritical impregnation, utilization of elemental composition determination using energy dispersive analysis of X-ray (EDAX) was carried out while performing TEM. Ni and Mo were detected at two arbitrary points of NiMo-SCF and their representative EDAX spectra are provided in Figures 9 and 10. The quantitative analysis of different elements showed 2.93 and 2.71 wt % for the Ni and 7.63 and 6.77 wt % for the Mo content in the two arbitrary chosen points. It is important to realize that the Ni/Mo ratio in the two arbitrary selected points is 0.384 and 0.400 which are very compatible. The obtained EDAX spectra of the two arbitrary points of the NiMo-SCF sample show images with no significant change in relative intensities. The EDAX results provide strong indication that most of the Ni and Mo in the NiMo-SCF are uniformly distributed in the Al_2O_3 support.

From the results of X-ray, oxygen chemisorption and EDAX analyses, it is likely possible to draw a general conclusion that the observed high and uniform dispersion for the NiMo-SCF catalyst is related to the morphology of the

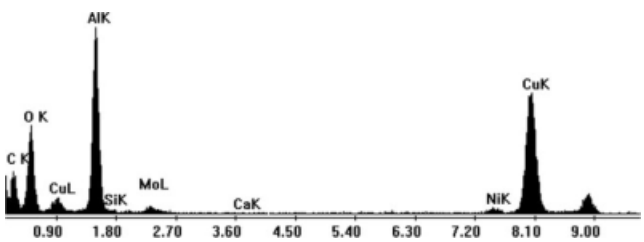

Figure 10. EDAX spectrum of E8-2 point of the NiMo-SCF catalyst (Figure 8).

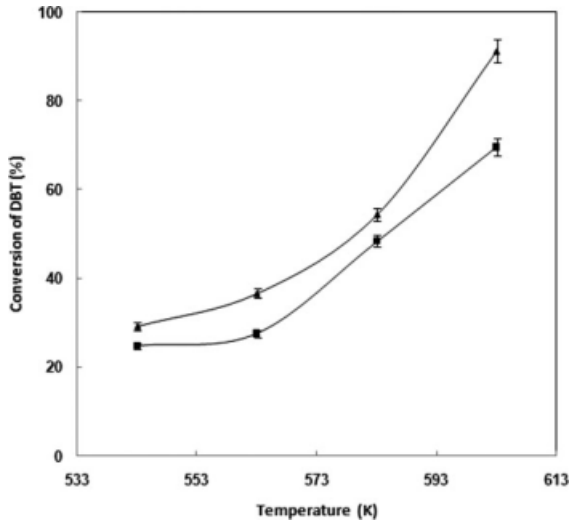

Figure 11. Conversion of DBT as a function of the reaction temperature.

(▲), NiMo-SCF catalyst; (■), NiMo-COM catalyst; P = 20 bar; catalyst weight = 0.5 g; H_2/feed ratio = 800 Nm^3/m^3; WHSV = 45 h^{-1}.

sulfided phase. MoS_2 crystallites on Al_2O_3 are expected to be shorter and to have less stacking of the layers[40,53,54] compared with those of NiMo-IMP catalyst. Smaller MoS_2 particles should have a greater number of active sites through increased exposure of MoS_2 crystallite edges. These suppositions were confirmed by comparing the amount of Mo active sites in Mo catalysts determined by oxygen chemisorption (Table 2).

Catalyst performance: HDS conversion and selectivity

In the present study, the catalytic performance of synthesized sulfided NiMo-SCFcatalyst in terms of conversion and selectivity was examined in the HDS of DBT; DBT was chosen as the hydrocarbon model compound because it is one of the most refractory sulfur compounds in gas oil. For comparison purposes, commercial catalyst (NiMo-COM) was also evaluated in the HDS of DBT.

Figure 11 shows the conversion of DBT in the HDS using NiMo-SCFcatalyst and NiMo-COM catalyst as a function of temperature. The NiMo-SCFcatalyst shows higher conversion of DBT into BP and CHB at all temperatures. For instance, conversion of 91.3% was obtained using NiMo-SCF catalyst at 603 K in contrast to 69.6% for the NiMo-COM catalyst. This increased conversion may be explained in terms of higher obtained dispersed deposition of active phases which would lead to significant frequency factor enhancement in the reaction rate constant according to the

Table 3. Reaction Rate Constants for HDS of DBT (mol/g cat. min $\times 10^5$); P = 20 bar, Catalyst Weight = 0.5 g, H_2/Feed Ratio = 800 Nm^3/m^3, WHSV = 45 h^{-1}

Catalyst	543 K	563 K	583 K	603 K
NiMo-SCF	0.70	0.93	1.60	4.96
NiMo-COM	0.58	0.66	1.35	2.42

Table 4. Activation Energy and Frequency Factor for the NiMo-SCF and NiMo-COM Catalysts; P = 20 bar, T = 543–603 K, Catalyst Weight = 0.5 g, H_2/Feed Ratio = 800 Nm^3/m^3, WHSV = 45 h^{-1}

Catalyst	K_0 (mol/g cat. min)	E/R (K)
NiMo-SCF	1.15×10^8	10386
NiMo-COM	1.64×10^6	8158

Arrhenius' law. As the supporting evidence for this phenomenon, the calculated reaction rate constants of HDS at temperatures of 543–603 K are summarized in Table 3. The reaction rate constant for the NiMo-SCF at 603 K increased about 105% with respect to the NiMo-COM catalyst. As shown in Table 4, the activation energy and frequency factor for the newly synthesized and commercial catalyst were calculated. The results show that frequency factor and activation energy is 70 and 1.3 times higher for the new synthesized catalyst with respect to the commercial one. Even though the activation energy of the synthesized catalyst is moderately higher than the commercial catalyst which is considered to be a disadvantage, but the positive effect of frequency factor for the new catalyst is much higher on the reaction rate. This incentive may be explained via obtained high dispersion and uniform distribution of metal active phase on the support by supercritical impregnation method in which much higher reaction rate can be achieved using the provided active surface area. According to Arrhenius' law, increased frequency factor leads to higher number of effective collision that causes higher conversion of reactants.

In accordance with other studies,[55,56] the aromatic hydrogenation efficiency is defined as the selectivity of CHB to BP. As shown in Figure 12, the overall selectivity in terms of yield of two products increases slightly in the temperature range of 543–603 K for the NiMo-SCF catalyst. But for the NiMo-COM catalyst, it is increasing moderately with

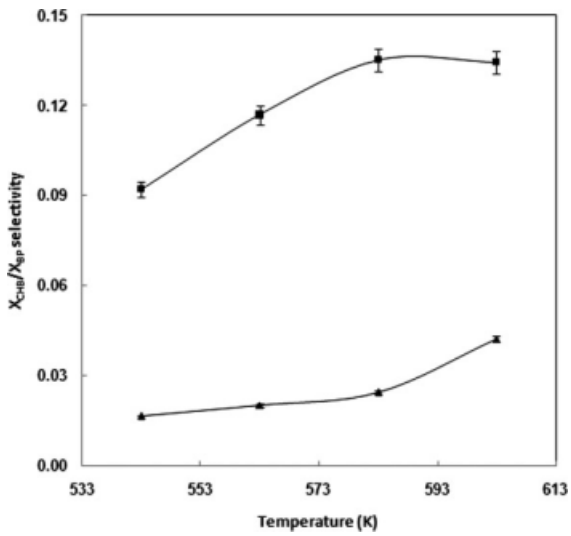

Figure 12. Variation of X_{CHB}/X_{BP} selectivity with temperature during HDS of DBT.

(▲), NiMo-SCF catalyst; (■), NiMo-COM catalyst; P = 20 bar; catalyst weight = 0.5 g; H_2/feed ratio = 800 Nm^3/m^3; WHSV = 45 h^{-1}.

increasing temperature until it reaches 593 K and becomes constant with subsequent increase of temperature up to 603 K as shown in Figure 12. The results demonstrate that the CHB/BP selectivity is lower using the synthesized catalyst with respect to the commercial catalyst. The results clearly indicate that the BP is the main product of HDS of DBT and indicates that the DDS is preferred on the NiMo catalysts. This route is preferred to HYD followed by desulfurization at all temperatures. This can be explained by looking at the different active sites necessary for DDS and HYD. The DDS route is generally believed to require sulfur vacancies on the catalyst surface, where the cleavage of C—S bond and the formation of H_2S can occur. Hydrogen disulfide then most probably adsorbs strongly on these sites and affects the DDS path. The HYD route is believed to proceed through the surface reaction of DBT on strong Brönsted acid active sites[57] followed by hydrogenation reaction with adsorbed H_2 on the adjacent active sites. Hence, it seems that H_2S affects mainly the DDS route while HYD is inhibited much less and this is more pronounced with increasing temperature. The observed increase in CHB/BP ratio is the result of this effect.

The inhibitive effect of aromatics on the HDS of DBT was studied by the addition of toluene to the feed mixture. The reaction rate constant of HDS at toluene concentration range of 0–20 wt % in feed at 583 K is summarized in Table 5. The conversion profile of DBT in the reactions with different amount of toluene is presented in Figure 13. A small addition of toluene decreases the conversion and the inhibition effect is getting stronger with the increasing amount of aromatics.[38,58,59] The results of Figure 13 show that the inhibition effect of synthesized NiMo-SCFcatalyst is lower than the commercial catalyst. This can be ascribed as another advantage for the newly developed catalyst. The effect of toluene clearly seems to be the suppression of the hydrogenation properties of the catalyst. The deactivation of the hydrogenolysis sites does not play a paramount role here and it can be speculated that the competition between toluene and DBT for the hydrogenation sites governs the importance of the different HDS pathways. This leads to a decrease of conversion of DBT.

Based on the physical/chemical characterization and activity evaluation of NiMo-SCF, NiMo-IMP and NiMo-COM catalysts, one can conclude that preparation of catalyst via supercritical deposition method, lead to a high dispersion of the metal species on the support. It is well accepted that high dispersion of Ni and Mo species on the support surface is essential for preparation of high performance HDS catalysts.

Conclusion

The synthesis of NiMo-SCF catalyst using a new impregnation method in the SC-CO_2-methanol solution resulted in higher conversion of HDS of DBT because of the following main phenomenon. Since supercritical medium has special fluid properties such as high diffusivity, low viscosity, and low surface tension, therefore, deposition of metals occurs with higher dispersion and uniformity on the support, which consequently results in much higher available active surface area on the catalyst. Thus, higher active surface area provides higher activity of the catalyst. Moreover, higher dispersion of catalytic metal with much reduced particle size results in less needed amount of metal and also avoids the undesirable particle agglomeration.

As a function of conversion and temperature in the HDS of DBT, the Al_2O_3 supported NiMo catalyst prepared by supercritical carbon dioxide deposition method to be more effective than the commercial industrial catalyst. In addition, 1.1 wt % less Mo was used in the new catalyst with respect to the commercial catalyst due to higher dispersion and uniformity of the active metallic phase. This saving in metal consumption becomes very cost effective in the case of expensive metals such as platinum, palladium, and rhenium which are usually being used in the petroleum processing.

Table 5. Reaction Rate Constants for HDS of DBT in *n*-Heptane-Toluene Mixture (mol/g cat. Min × 10^5); T = 583 K, P =20 bar, Catalyst Weight = 0.5 g, H_2/Feed Ratio = 800 Nm^3/m^3, WHSV = 45 h^{-1}

Toluene Concentration (wt %)	0	10	20
NiMo-SCF	1.60	1.39	1.06
NiMo-COM	1.35	0.95	0.85

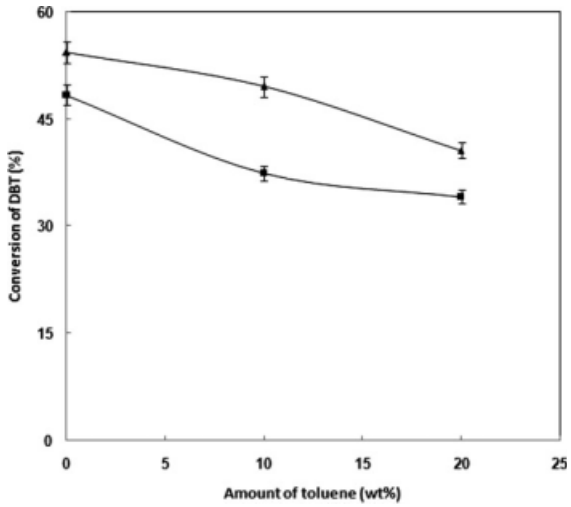

Figure 13. Conversion of DBT as a function of the amount of toluene in the feed.

(▲), NiMo-SCF catalyst; (■), NiMo-COM catalyst; T = 583 K; P = 20 bar; catalyst weight = 0.5 g; H_2/feed ratio = 800 Nm^3/m^3; WHSV = 45 h^{-1}.

Acknowledgments

The financial support provided for this project by the Research Institute of Petroleum Industry of Iran (RIPI) and Isfahan University of Technology (IUT) was gratefully acknowledged. The helpful technical assistance offered by Mr. M. A. Attarnejad and Mrs. A. Tofigh was appreciated.

Notation

BJH = Barret-Joyner-Halenda
BP = biphenyl
C_{BP} = concentration of biphenyl (mol/lit)
C_{CHB} = concentration of cyclohexylbenzene (mol/lit)
CHB = cyclohexylbenzene
CS_2 = carbon disulfide
D_p = average pore diameter (nm)
D_z = axial dispersion coefficient (m^2/sec)

DBT = dibenzothiophene
DDS = direct desulfurization route
E = activation energy (J/mol)
EDAX = energy dispersive analysis of X-ray
EDF = equilibrium deposition filtration
F = feed rate of DBT (mol/min)
HDS = hydrodesulfurization
HYD = hydrogenation reaction pathway
k_o = frequency factor (mol/g cat. min)
k_{HDS} = reaction rate constant of HDS (mol/g cat. min)
N_{Pe} = Peclet number
P = pressure (bar)
P_0 = ambient pressure (bar)
R = universal gas constant (J/mol.K)
S_{BET} = specific area by BET method (m^2/g)
S_o = overall selectivity
SCF = supercritical fluid
SC-CO_2 = supercritical carbon dioxide
T = temperature (K)
TCD = thermoconductivity detector
TEM = transmission electron microscopy
TPD = temperature programmed desorption
TPR = temperature programmed reduction
V_p = pore volume (m^3/g)
W = catalyst weight (g)
WHSV = weight hourly space velocity (1/h)
X = mole fractional conversion of DBT
X_{CHB} = mole fractional conversion of DBT to CHB
X_{BP} = mole fractional conversion of DBT to BP
XRD = X-ray diffraction

Literature Cited

1. Chen J, Ring Z. HDS reactivities of dibenzothiophenic compounds in a LC-finer LGO and H_2S/NH_3 inhibition effect. *Fuel*. 2004;83: 305–313.
2. Perot G. Hydrotreating catalysts containing zeolites and related materials-mechanistic aspects related to deep desulfurization. *Catal Today*. 2003;86:111–128.
3. Cejka J. Organized mesoporous alumina: synthesis, structure and potential in catalysis. *Appl Catal A*. 2003;254:327–338.
4. Saih Y, Segawa K. Tailoring of alumina surfaces as supports for NiMo sulfide catalysts in the ultra deep hydrodesulfurization of gas oil: case study of TiO_2-coated alumina prepared by chemical vapor deposition technique. *Catal Today*. 2003;86:61–72.
5. Song C, Reddy KM. Mesoporous molecular sieve MCM-41 supported Co-Mo catalyst for hydrodesulfurization of dibenzothiophene in distillate fuels. *Appl Catal A*. 1999;176:1–10.
6. Reddy KM, Wei B, Song C. Mesoporous molecular sieve MCM-41 supported Co-Mo catalyst for hydrodesulfurization of petroleum resids. *Catal Today*. 1998;43:261–272.
7. Wang A, Wang Y, Kabe T, Chen Y, Ishihara A, Qian W. Hydrodesulfurization of dibenzothiophene over siliceous MCM-41-supported catalysts I. sulfided Co-Mo catalysts. *J Catal*. 2001;199:19–29.
8. Cheng M, Kumata F, Saito T, Komatsu T, Yashima T. Preparation and characterization of Mo catalysts over AlMCM-41/γ-Al_2O_3 extruded supports. *Appl Catal A*. 1999;183:199–208.
9. Venezia AM, Parola VL, Deganello G, Cauzzi D, Leonardi G, Predieri G. Influence of the preparation method on the thiophene HDS activity of silica supported CoMo catalysts. *Appl Catal*. 2002;229: 261–271.
10. Papadopoulou CH, Vakros J, Matralis HK, Kordulis CH, Lycourghiotis A. On the relationship between the preparation method and the physicochemical and catalytic properties of the CoMo/γ-Al_2O_3 hydrodesulfurization catalysts. *J Colloid Interface Sci*. 2003;261: 146–153.
11. Sampieri A, Pronier S, Blanchard J, Breysse M, Brunet S, Fajerwerg K, Louis C, Pérot G. Hydrodesulfurization of dibenzothiophene on MoS_2/MCM-41 and MoS_2/SBA-15 catalysts prepared by thermal spreading of MoO_3. *Catal Today*. 2005;107–108:537–544.
12. Mariño F, Descorme C, Duprez D. Supported base metal catalysts for the preferential oxidation of carbon monoxide in the presence of excess hydrogen (PROX). *Appl Catal B*. 2005;58:175–183.
13. Carmo M, Paganin VA, Rosolen JM, Gonzalez ER. Alternative supports for the preparation of catalysts for low-temperature fuel cells: the use of carbon nanotubes. *J Power Sources*. 2005;142:169–176.
14. Cabañas A, Long DP, Watkins JJ. Deposition of gold films and nanostructures from supercritical carbon dioxide. *Chem Mater*. 2004;16:2028–2033.
15. Hunde ET, Watkins JJ. Reactive deposition of cobalt and nickel films from their metallocenes in supercritical carbon dioxide solution. *Chem Mater*. 2004;16:498–503.
16. Blackburn J, Long DP, Cabañas A, Watkins JJ. Deposition of conformal copper and nickel films from supercritical carbon dioxide. *Science*. 2001;294:141–145.
17. Cabañas A, Blackburn JM, Watkins JJ. Deposition of Cu films from supercritical fluids using Cu(I) β-diketonate precursors. *Microelectron Eng*. 2002;64:53–61.
18. Cabañas A, Shan X, Watkins JJ. Alcohol-assisted deposition of copper films from supercritical carbon dioxide. *Chem Mater*. 2003;15: 2910–2916.
19. Saquing CD, Cheng TT, Aindow M, Erkey C. Preparation of platinum/carbon aerogel nanocomposites using a supercritical deposition method. *J Phys Chem B*. 2004;108:7716–7722.
20. Zhang Y, Kang D, Saquing C, Aindow M, Erkey C. Supported platinum nanoparticles by supercritical deposition. *Ind Eng Chem Res*. 2005;44:4161–4164.
21. Zhang Y, Erkey C. Preparation of platinum-nafion-carbon black nanocomposites via a supercritical fluid Route as electrocatalysts for proton exchange membrane fuel cells. *Ind Eng Chem Res*. 2005;44: 5312–5317.
22. Zhang Y, Kang D, Aindow M, Erkey C. Preparation and characterization of ruthenium/carbon aerogel nanocomposites via a supercritical fluid route. *J Phys Chem B*. 2005;109:2617–2624.
23. Ghoreishi SM, Sharifi S. Modeling of supercritical extraction of Mannitol from plane tree leaf. *J Pharmaceut Biomed*. 2001;24: 1037–1048.
24. Michael AC, Wightman RM. Microelectrodes coated with ionically conducting polymer membranes for voltammetric detection in flowing supercritical carbon dioxide. *Anal Chem*. 1989;61:270–272.
25. Sun Z, Liu Z, Han B, Miao S, Miao Z, An G. Decoration carbon nanotubes with Pd and Ru nanocrystals via an inorganic reaction route in supercritical carbon dioxide-methanol solution. *J Coll Int Sci*. 2006;304:323–328.
26. Abbott AP, Harper JC. Electrochemical investigations in supercritical carbon dioxide. *J Chem Soc Faraday Trans*. 1996;92:3895–3898.
27. Abbott AP, Griffiths GA, Harper JC. Conductivity of long chain quaternary ammonium electrolytes in cyclohexane. *J Chem Soc Faraday Trans*. 1997;93:577–582.
28. Warzinski RP. Supercritical-fluid solubilization of catalyst precursors: the solubility and phase behavior of molybdenum hexacarbonyl in supercritical carbon dioxide and application to the direct liquefaction of coal. *J Supercritical Fluids*. 1992;5:60–71.
29. Houalla M, Broderick DH, Sapre AV, Naga NK, de Beer VHJ, Gates BC, Kwart H. Hydrodesulfurization of methyl-substituted dibenzothiophenes catalyzed by sulfided CoMo/γ-Al_2O_3. *J Catal*. 1980;61:523–527.
30. Lanure-Meille V, Schulz E, Lemaire M, Vrinat M. Effect of experimental parameters on the relative reactivity of dibenzothiophene and 4-methyldibenzothiophene. *Appl Catal A*. 1995;131:143–157.
31. Sie ST. Miniaturization of hydroprocessing catalyst testing systems: theory and practice. *AlChE J*. 1996;42:3498–3507.
32. Bej SK, Dabral RP, Gupta PC, Mittal KK, Sen GS, Kapoor VK, Dalai AK. Studies on the performance of a microscale trickle bed reactor using different sizes of diluents. *Energy Fuels*. 2000;14:701–705.
33. Egorova M, Prins R. Mutual influence of the HDS of dibenzothiophene and HDN of 2-methylpyridine. *J Catal*. 2004;221:11–19.
34. Maity SK, Rana MS, Bej SK, Ancheyta Juarez J, Murali Dhar G, Prasada Rao TSR. Studies on physico-chemical characterization and catalysis on high surface area titania supported molybdenum hydrotreating catalysts. *Appl Catal*. 2001;205:215–225.
35. Rao KSP, Ramakrishna H, Murali Dhar G. Catalytic functionalities of WS2/ZrO_2. *J Catal*. 1992;133:146–152.
36. Steiner P, Blekkan EA. Catalytic hydrodesulfurization of a light gas oil over a NiMo catalyst: kinetics of selected sulfur components. *Fuel Process Technol*. 2002;79:1–12.

37. Shimada H, Sato T, Yoshimura Y, Hiraishi J, Nishijima A. Support effect on the catalytic activity and properties of sulfided molybdenum catalysts. *J Catal*. 1988;110:275–284.
38. Yue Y, Sun Y, Gao Z. Disordered mesoporous KIT-1 as a support for hydrodesulfurization catalysts. *Catal Lett*. 1997;47:167–171.
39. Silva-Rodrigo R, Calderón-Salasa C, Melo-Bandaa JA, Domínguezb JM, Vázquez-Rodríguezb A. Synthesis, characterization and comparison of catalytic properties of NiMo and NiW/Ti-MCM-41 catalysts for HDS of thiophene and HVGO. *Catal Today*. 2004;98: 123–129.
40. Herrera JM, Reyes J, Roquero P, Klimova T. New hydrotreating NiMo catalysts supported on MCM-41 modified with phosphorus. *Microporous Mesoporous Mater*. 2005;83:283–291.
41. Prins, R. Characterization of catalytic materials. In: Wachs IE, Fitzpatrick LE, editors. *Supported Metal Sulfides*. Boston: MA, Butterworth-Heinemann, 1992:109–127.
42. Zepeda TA, Halachev T, Pawelec B, Nava R, Klimova T, Fuentes GA, Fierro JLG. Hydrodesulfurization of dibenzothiophene over CoMo/HMS and CoMo/Ti-HMS catalysts. *Cata Communications*. 2006;7:33–41.
43. Noronha FB, Baldanza MAS, Schmal M. CO and NO adsorption on alumina-Pd-Mo catalysts: effect of the precursor salts. *J Catal*. 1999;188:270–280.
44. Abello MC, Gomez MF, Ferreti O. Mo/γ-Al_2O_3 catalysts for the oxidative dehydrogenation of propane: effect of Mo loading. *Appl Catal A*. 2001;207:421–431.
45. Li J, Jacobs G, Zhang Y, Das T, Davis BH. Fischer-Tropsch synthesis: effect of small amounts of boron, ruthenium and rhenium on Co/TiO_2 catalysts. *Appl Catal A*. 2002;223:195–203.
46. Brito JL, Laine J. Reducibility of Ni-Mo/Al_2O_3 catalysts: a TPR study. *J Catal*. 1993;139:540–550.
47. López Cordero R. López Agudo A. Effect of water extraction on the surface properties of Mo/Al_2O_3 and NiMo/Al_2O_3 hydrotreating catalysts. *Appl Catal A*. 2000;202:23–25.
48. López Cordero R, Gil Llambias FJ, López Agudo A. Temperature-programmed reduction and zeta potential studies of the structure of Mo/$O_3Al_2O_3$ and Mo/O_3SiO_2 catalysts effect of the impregnation pH and molybdenum loading. *Appl Catal*. 1991;74:125–136.
49. Klimova T, Calderón M, Ramírez J. Ni and Mo interaction with Al-containing MCM-41 support and its effect on the catalytic behavior in DBT hydrodesulfurization. *Appl Catal A*. 2003;240:29–40.
50. Dufresne P, Payen E, Grimblot J, Bonnele JP. Study of nickel-molybdenum-.gamma.-aluminum oxide catalysts by x-ray photoelectron and Raman spectroscopy: comparison with cobalt-molybdenum-gamma-aluminum oxide catalysts. *J Phys Chem*. 1981;85:2344–2351.
51. Damyanova S, Spojakina A, Jiratova K. Effect of mixed titania-alumina supports on the phase composition of NiMo/$TiO_2Al_2O_3$ catalysts. *Appl Catal A*. 1995;125:257–269.
52. Li X, Wang A, Wang Y, Chen Y, Liu Y, Hu Y. Hydrodesulfurization of dibenzothiophene over Ni-Mo sulfides supported by proton-exchanged siliceous MCM-41. *Catal Lett*. 2002;84:107–113.
53. Gutiérrez OY, Valencia D, Fuentes GA, Klimova T. Mo and NiMo catalysts supported on SBA-15 modified by grafted ZrO_2 species: synthesis, characterization and evaluation in 4,6-dimethyldibenzothiophene hydrodesulfurization. *J Catal*. 2007;249:140–153.
54. Sampieri A, Pronier S, Blanchard J, Breysse M, Brunet S, Fajerwerg K, Louis C, Pérot G. Hydrodesulfurization of dibenzothiophene on MoS_2/MCM-41 and MoS_2/SBA-15 catalysts prepared by thermal spreading of MoO_3. *Catal Today*. 2005;107–108:537–544.
55. Landau MV, Berger D, Herskowitz M. Hydrodesulfurization of methyl-substituted dibenzothiophenes: fundamental study of routes to deep desulfurization. *J Catal*. 1996;159:236–245.
56. Ho TC, Sobel JE. Kinetics of dibenzothiophene hydrodesulfurization. *J Catal*. 1991;128:581–584.
57. Nagai M, Sato T, Aiba A. Poisoning effect of nitrogen compounds on dibenzothiophene hydrodesulfurization on sulfided NiMo/Al2O3 catalysts and relation to gas-phase basicity. *J Catal*. 1986;97:52–58.
58. Robinson WRAM, van Veen JAR, de Beer VHJ, van Santen RA. Development of deep hydrodesulfurization catalysts: II. NiW, Pt and Pd catalysts tested with (substituted) dibenzothiophene. *Fuel Process Technol*. 1999;61:103–116.
59. Jongpatiwut S, Li Z, Resasco DE, Alvarez WE, Sughrue EL, Dodwell GW. Competitive hydrogenation of poly-aromatic hydrocarbons on sulfur-resistant bimetallic Pt-Pd catalysts. *Appl Catal A*. 2004; 262:241–253.

Manuscript received Oct. 9, 2008, and revision received Jan. 16, 2009.